UDK 686.4:544.022.6:620.193.95
Original scientific article/Izvirni znanstveni članek

ISSN 1580-2949
MTAEC9, 57(4)341(2023)

MICROSTRUCTURE AND HIGH-TEMPERATURE WEAR BEHAVIOR OF FE-BASED AMORPHOUS COATINGS BY LASER CLADDING

MIKROSTRUKTURA IN VISOKOTEMPERATURNA MEHANSKA OBRABA AMORFNIH PREVLEK NA OSNOVI ŽELEZA, IZDELANIH Z LASERSKIM NAPRŠEVANJEM

Lu Xie[1*], Yueming Wang[2], Jianlin Yang[1], Chenlong Li[2], Xuhang Han[2], Jie Huang[2]

[1]School of Management Engineering, Jiangsu Urban and Rural Construction Vocational College, Changzhou 213147, China
[2]Hunan Provincial Key Defense Laboratory of High Temperature Wear-resisting Materials and Preparation Technology, Hunan University of Science and Technology, Xiangtan 411201, PR China

Prejem rokopisa – received: 2023-01-24; sprejem za objavo – accepted for publication: 2023-06-04

doi:10.17222/mit.2023.803

FeCrMoCB amorphous coatings were prepared on 316 stainless steel via an amorphous powder. Scanning electron microscopy (SEM), energy-dispersive spectroscopy (EDS), and X-ray diffraction (XRD) were used to analyze the microstructure, composition, and phase structure of the coatings. Hardness and friction wear testers were applied to investigate the microhardness and wear behavior of the coatings. Results show that the $Cr_{23}C_6$, $Cr_{15}Fe_7C_6$ and Fe_3Mo crystal phases appeared after laser cladding relative to the complete amorphous powder, and the amorphous phase fraction of the coating was calculated up to 68.4 % using the Verdon method. The coating exhibited a dominating adhesive wear mechanism under room temperature (RT) and transformed to a fatigue wear mechanism as wear test temperature increased to 600 °C. As the temperature was elevated from RT to 600 °C, the wear rate increased from 26×10^{-6} mm^3/N·m to 79×10^{-6} mm^3/N·m. The laser-cladded Fe-based amorphous coating exhibited much stronger wear performance than the 316 stainless steel, even the wear rate reached one third of that of steel.

Keywords: laser cladding, Fe-based amorphous coating, test temperature, wear behavior

V članku avtorji opisujejo izdelavo in karakterizacijo amorfnih prevlek FeCrMoCB na podlagi iz nerjavnega jekla vrste 316. Izdelava prevlek je potekala z laserskim napršavanjem amorfnega prahu. S pomočjo vrstične elektronske mikroskopije (SEM), energijske disperzijske spektroskopije (EDS) in rentgenske difrakcije (XRD) so analizirali mikrostrukturo ter določili kemijsko in fazno sestavo izdelanih prevlek. Obrabno odpornost prevlek so ocenili z meritvami trdote in testne naprave za določitev obrabe zaradi trenja. Rezultati preiskav so pokazali, da so med laserskim napršavanju nastale kristalinične faze $Cr_{23}C_6$, $Cr_{15}Fe_7C_6$ in Fe_3Mo, S pomočjo Verdonove metode pa so ugotovili, da je nastali delež amorfne faze v prevlekah do približno 68,4 %. Prevladujoči obrabni mehanizem do sobne temperature je adhezivna obraba in prehaja v mehanizem obrabe zaradi utrujanja materiala do temperature 600 °C. Od sobne temperature pa do 600 °C je hitrost obrabe narasla s 26×10^{-6} mm^3/N·m na 79×10^{-6} mm^3/N·m. Izdelana lasersko napršena amorfna prevleka na osnovi železa je mnogo bolj odporna proti obrabi kot podloga iz jekla vrste 316 in je ocenjeno za do tretjino manjša.

Ključne besede: lasersko nanašanje, amorfne prevleke na osnovi železa, temperatura preizkusa, visokotemperaturna obraba prevleke

1 INTRODUCTION

Amorphous alloys have gained increasing attention because of their high hardness and excellent mechanical properties.[1–5] Among those amorphous alloys, Fe-based amorphous alloys have attracted much interest due to the relative low cost and high wear resistance for industrial applications.[6–22] However, the production and application of Fe-based amorphous alloys were restricted because of dimension limitations and room-temperature brittleness.[23–27]

An amorphous coating, as an alternative form of amorphous alloy, can overcome the dimensional limitation and avoid the room-temperature brittleness of an amorphous block, receiving more and more attention in surface engineering.[28–32] Various methods have been applied to fabricate Fe-based amorphous coatings, including plasma spraying, high-velocity oxygen fuel (HVOF) spraying, laser cladding and so on. The microstructure, mechanical properties, and elevated-temperature tribological performance of an Fe-Cr-Mo-W-C-B-Y amorphous coating that was prepared via activated combustion high-velocity air fuel (AC-HVAF) spraying was investigated by Liang et al.[33] The wear mechanism changed from abrasive wear accompanied by delamination and adhesive wear to the delamination and adhesive ones as temperature rose from 293 K to 673 K. The evolutions of microstructure, fracture toughness and the sliding-wear behaviors of APS $Fe_{43}Cr_{16}Mo_{16}(C,B,P)_{25}$ amorphous coatings, which were fabricated by air plasma spraying (APS) with various powers, were investigated by Cheng et al.[34]

Laser cladding has gained much attention due to super high bonding strength and coating density relative

*Corresponding author's e-mail:
xielucsu@163.com

to other fabricating technologies. Lu et al.[35] prepared crack-free Fe-based amorphous coatings by laser cladding, which adopted a triple laser scanning strategy. The deposited Fe-based amorphous coating displayed a stable wear process and a low wear loss for a much longer service time under dry-sliding wear conditions, which was much superior to 45 steel. Fe-Cr-Si-P/La_2O_3 amorphous composite coatings were prepared on 304L substrates by laser cladding, as reported by Lu et al.[36] The effects of La_2O_3 content on the microstructure, phase composition and microhardness of composite coatings were investigated. Hou et al.[37] synthesized a novel amorphous composite coating on 3Cr13 stainless steel by laser cladding an Fe-Cr-Mo-Co-C-B amorphous powder. The highest hardness of the cladding layer was 1179 $HV_{0.5}$, which was about 6 times that of the 3Cr13 stainless-steel substrate (200 $HV_{0.5}$). As a result, the wear resistance of the substrate was greatly improved by the cladding layer.

However, there are few reports on the effects of temperature on the wear behavior of a laser-cladded Fe-based amorphous coating, especially the high-temperature wear friction behavior was rarely studied. As a result, an FeCrMoCB amorphous coating was deposited on 316 stainless steel by laser cladding. And systematic study was carried out to investigate the effects of various test temperatures on the microstructure and wear properties of the Fe-based amorphous coating.

2 EXPERIMENTAL

2.1 Synthesis of powder and coating

A commercial Fe-based amorphous powder (Liquid metal company, USA) with a particle size of 16–54 μm was adopted to fabricate the Fe-based amorphous coatings. The nominal composition of the feedstock is listed in **Table 1**. The 316 stainless steel plates with dimensions of 100 × 30 × 10 mm^3 were selected as substrates. The substrates were sand blasted to activate the surface and remove the grease for a higher bonding strength. The substrate surface roughness (R_a) was controlled to about 5 μm. Subsequently, they were ultrasonically cleaned and dried in air. The spray experiments were conducted via a commercially available laser system (LDF-3000, Laserline, Germany), an operating optical fiber (600 μm, Laserline, Germany), a laser integrated control system (S7-1200, Siemens, Germany), a laser-cladding coaxial powder-feeding nozzle (OTS-2, Laserline, Germany) and a water-cooling system and a powder-feeding system. The pressure of powder feeding gas (N_2) and the height of the nozzle from the sample surface was 6 Mpa and 12–14 mm, respectively. The nozzle was made of red copper. The laser cladding parameters are listed in **Table 2**.

Table 1: Nominal composition of the Fe-based amorphous powder

Element	Cr	C	Mo	B	Fe
FeCrMoCB	26.0	2.3	17.0	2.1	Bal.

Table 2: Laser cladding parameters from Fe-based amorphous powder

Element	Laser power /kW	Scanning speed /(mm·s^{-1})	Spot diameter /mm	Overlapping ratio /%
FeCrMoCB	1.4	12	3	50

2.2 High-temperature friction and wear testing

Dry sliding tribological properties of the laser cladded Fe-based amorphous coatings were investigated by a reciprocating friction-and-wear tester (GF-I, Lanzhou ZhongkeKaihua Technology Development Co., Ltd., China) in accordance with ASTM D6279-2003 (2013) at room temperature, 200 °C, 400 °C and 600 °C. Si_3N_4 balls with diameter of 6 mm were selected as the counterparts. New balls were used for each test. All the coating samples were grinded and polished to a mirror surface with roughness of R_a = 1 μm. The wear debris was collected after wear testing for subsequent observation.

The load, rotating speed, friction time and sliding distance were 60 N, 600 min^{-1}, 30 min and 5 mm, respectively. The wear rate *Ws* of the coating can be estimated using the equation of $Ws = V/DL$, where V is the volume loss, D is the sliding distance, and L is the load applied to the specimen. The volume loss $V = m/\rho$, where ρ is the density of the coating material, m is the mass loss measured after each test. The surfaces of the coatings before and after the wear friction were characterized by SEM.

2.3 Microstructural characterization

The surface morphologies of the feedstock, laser-cladded coatings, wear debris, friction and wear surfaces of the amorphous coating and Si_3N_4 dual grinding balls were characterized using a scanning electron microscope (TescanMira4, Tescan Orsay Holding, Czech Republic). The phase structure was studied by X-ray diffraction (XRD, Rigaku D/max-2550VB) using Cu-K_α radiation. The diffraction angle was from 20° to 80°. The coating porosity was evaluated using the Image Pro-Plus 6.0 software. At least ten cross-sectional SEM images at a magnification of 1000 times were randomly selected for the porosity calculation of each coating.

3 RESULTS AND DISCUSSION

3.1 Microstructural characterization

The particle size distribution of the Fe-based amorphous powder ranging from approximately 15 μm to 80 μm (most of particles ranged from 35 μm to 40 μm) is suitable for laser cladding, as shown **in Figure 1a**. Spherical and dense microstructures with few pores can be found as **Figure 1b** and **1c**. This kind of compact microstructure of feedstock is beneficial to obtain a uniform melting effect during the laser cladding. Finally, a

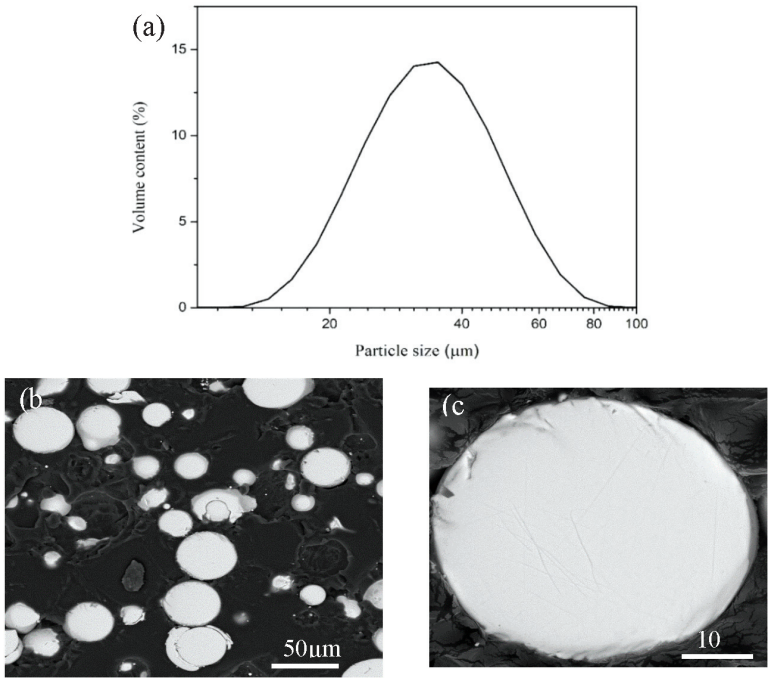

Figure 1: Particle size distribution and cross-section morphology of the Fe-based amorphous powder: a) particle size distribution, b) panorama morphology and c) high-magnification morphology of a single particle

coating with a homogeneous microstructure can be deposited.[38,39]

Figure 2 shows Fe, Cr, Mo, C and B element-map distributions on the cross-section of the powder particle. The main elements including Fe, Cr and Mo are homogeneously distributed in the particle. The composition homogeneity of the laser-cladded amorphous coating can be improved by this kind of powder.

Figure 3 shows the XRD patterns of Fe-based amorphous powder and coating. A broad diffused scattering peak appears between 40° and 50°, as shown in **Figure 3**, which is the typical pattern of an amorphous phase, indicating almost complete amorphization of the iron-based powder. Several sharp peaks appear in the XRD pattern of the coating, which is related to the formation of some crystal phases during laser cladding. The crystal phases were found to be $Cr_{23}C_6$, $Cr_{15}Fe_7C_6$ and Fe_3Mo via the MDI Jade. The amorphous phase fraction of the coating was about 68.4 %, after calculation using the Verdon method. The appearance of crystal phases

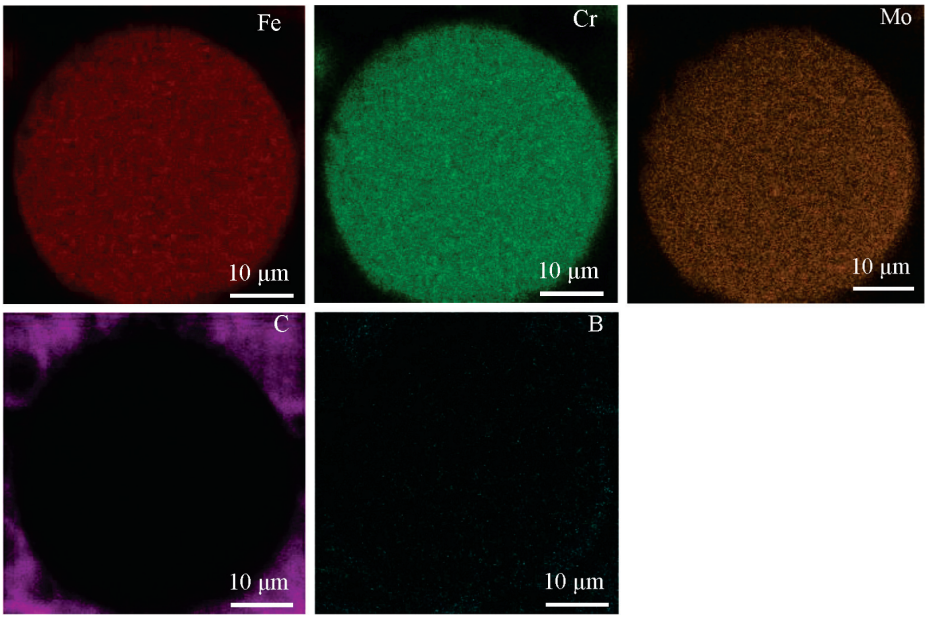

Figure 2: Fe, Cr, Mo, C and B element-map distributions on the cross-section of a single Fe-based amorphous particle

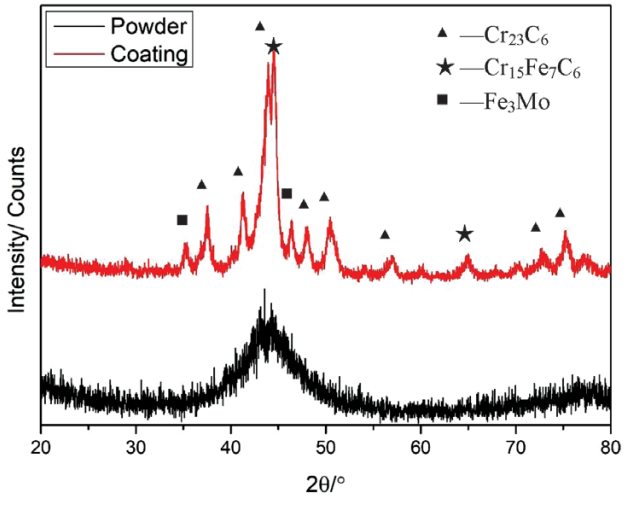

Figure 3: XRD patterns of the Fe-based amorphous powder and coating

can be ascribed to part of the powder being melted during the laser cladding, and then crystallization occurred in the subsequent cooling and solidification process. Moreover, a portion of crystallization of cladded coating occurred due to being heated during subsequent deposition.

Figure 4 shows the SEM photographs of the center and bottom of the cross-section of cladded Fe-based amorphous coating. From **Figure 4a** and **4b**, large amounts of crystalline grains appeared in the amorphous matrix, representing rectangular and triangular shapes. The three phases are indicated by the colors of light grey, white and dark grey, respectively. The interface morphology of the coating and substrate is shown in **Figure 4c** and **4d**. A planar layer appeared in the bonding region with a thickness of about 2 μm. With increasing distance from the surface of substrate, the planar layer was gradually restrained, and several columnar dendrites were formed. With increasing distance from substrate surface, the columnar dendrites transformed to ellipsoid grains. Subsequently, rectangular and triangular grains were precipitated at the center of the cladded coating as in **Figure 4a** and **4b**.

According to the classical theory of the rapid solidification, the phase and the morphology of material microstructure are basically related to the ratio of temperature gradient G to solidification rate R, i.e. G/R.[40,4] In the initial stage of laser cladding, the powder was melted by laser beam, and conducted the heat to the substrate surface, which led the metallurgical bonding of the coating and coating. In this condition, the G was large and R was small, therefore, the G/R was huge, leading the planar layer growth in the bonding area. With increasing distance from the substrate surface, the G/R decreased, and then the growth of dendrites and fine grains was sup-

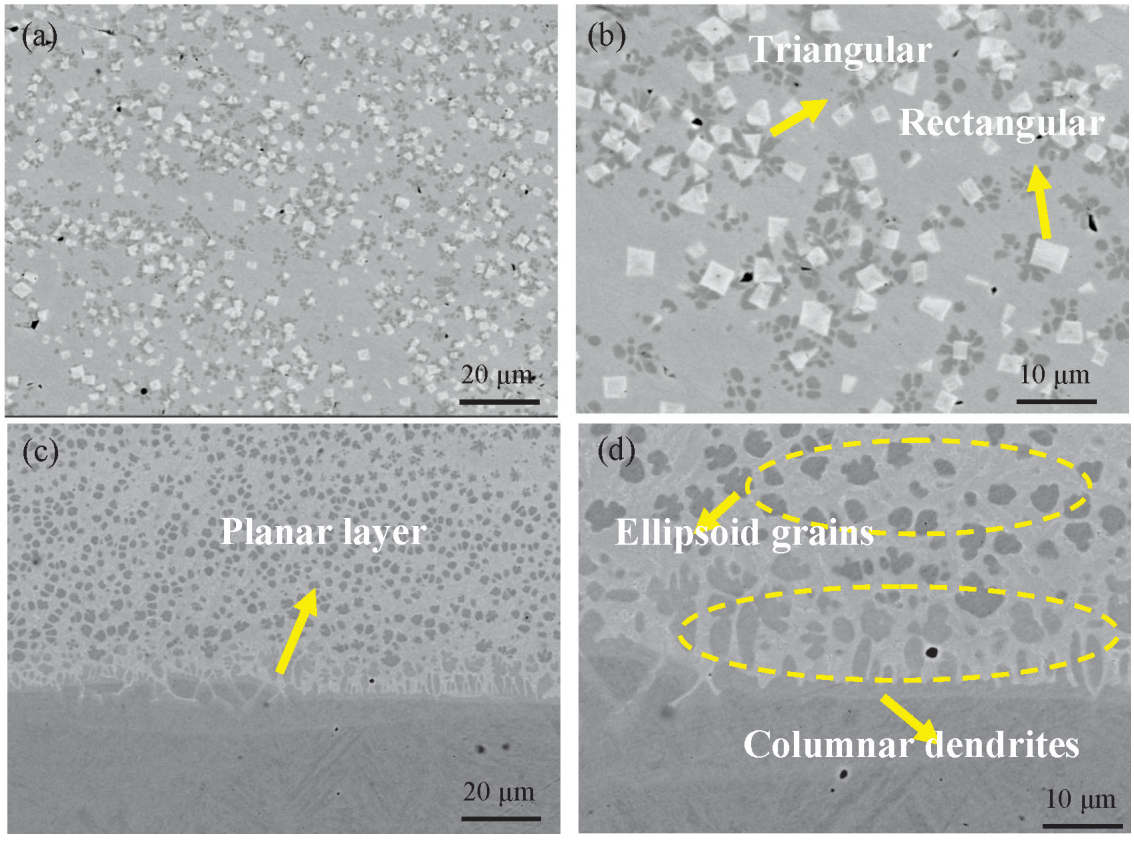

Figure 4: SEM photographs of the cross-section of Fe-based amorphous coating prepared by laser cladding: a) the center layer of the cladded Fe-based amorphous coating, b) magnified image of a), c) the bottom of the cladded Fe-based amorphous coating, d) magnified image of c)

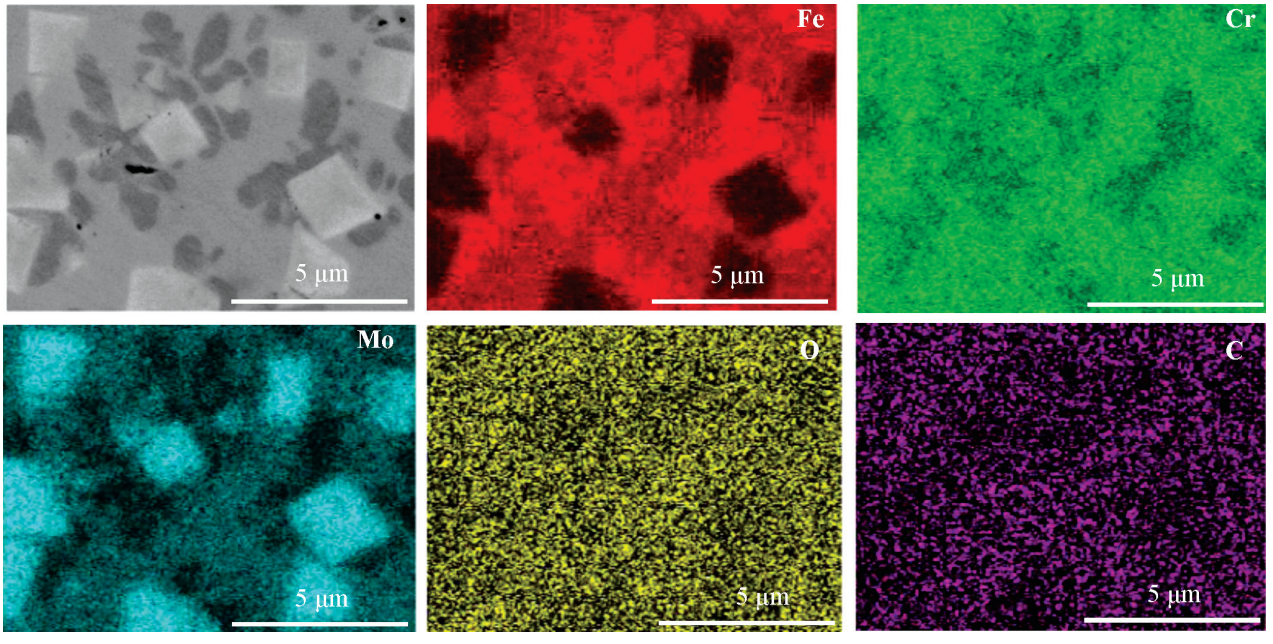

Figure 5: EDS mapping of the cross-section of the interior coating

pressed. Meanwhile, coarse ellipsoid grains, rectangular and triangular grains started to precipitate and grow.

Figure 5 shows EDS mapping of the cross-section of the interior coating. It should be noted that the white phase, dark phase and grey phase were the Mo-enriched area, the Fe-enriched area and the Cr-enriched area, respectively. Oxygen and carbon were uniformly distributed in the coating. As a result, the rectangular grains and ellipsoid grains were mainly Fe alloy and Mo alloy, respectively.

Figure 6 shows the EDS mapping of the interface of the coating and substrate. The result shows that the grey phase region is rich in Fe, while the white phase region is rich in Cr and Mo. This morphology indicates that as the laser cladding began, the *G*/*R* value was huge, resulting in large amounts of precipitation of Fe-based crystalline material. It is dominated by columnar dendrites near the substrate surface and ellipsoid grains in the centre coating, as the above results indicated. The transformation of morphology did not change the phase composi-

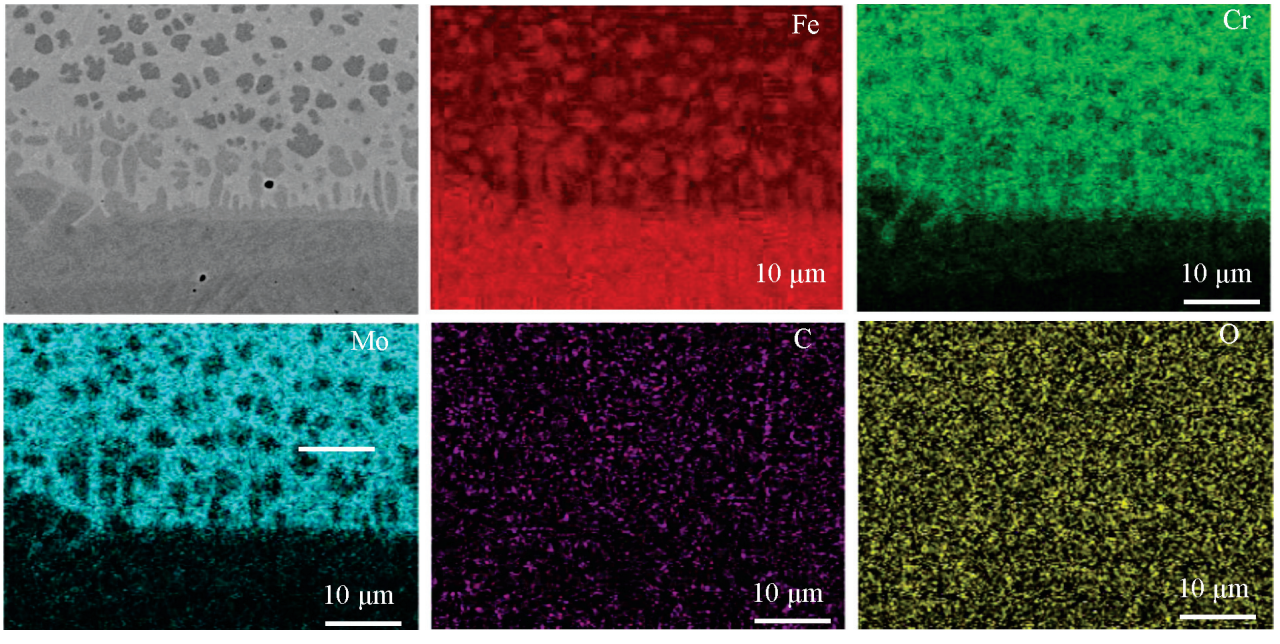

Figure 6: EDS mapping of the interface of coating and substrate

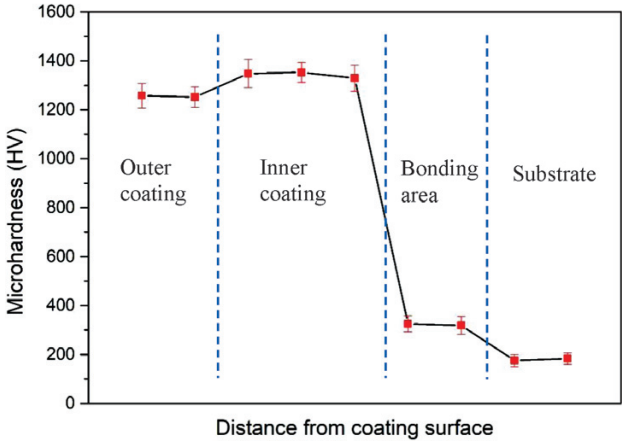

Figure 7: Microhardness of various areas from outer coating to steel substrate

tion according to the element-distribution result. Moreover, oxygen is uniformly distributed, indicating there was few preferential reactions between the metallic elements and oxygen.

3.2 Microhardness and wear behavior of iron-based amorphous coating

3.2.1 Microhardness

Microhardness of various areas from outer coating to the substrate can be found in **Figure 7**. The microhardness of the inner coating, outer coating, bonding area and steel substrate were approximately 1300 $HV_{0.1}$, 1250 $HV_{0.1}$, 300 $HV_{0.1}$ and 170 $HV_{0.1}$, respectively. The microhardness of the iron-based amorphous coating was much higher than that of steel substrate due to the atomic-structure randomness in the amorphous phase[42]. In addition, the hardness of outer coating was a little lower than that of inner one, which may be due to the residual thermal stress during laser cladding. Note here, tensile stress formed in the coating due to rapid solidification and shrinkage of the droplet in the process of laser cladding. The hardness of the bonding area was between those of the laser cladded coating and the steel substrate for being composed of the amorphous phase and the substrate.

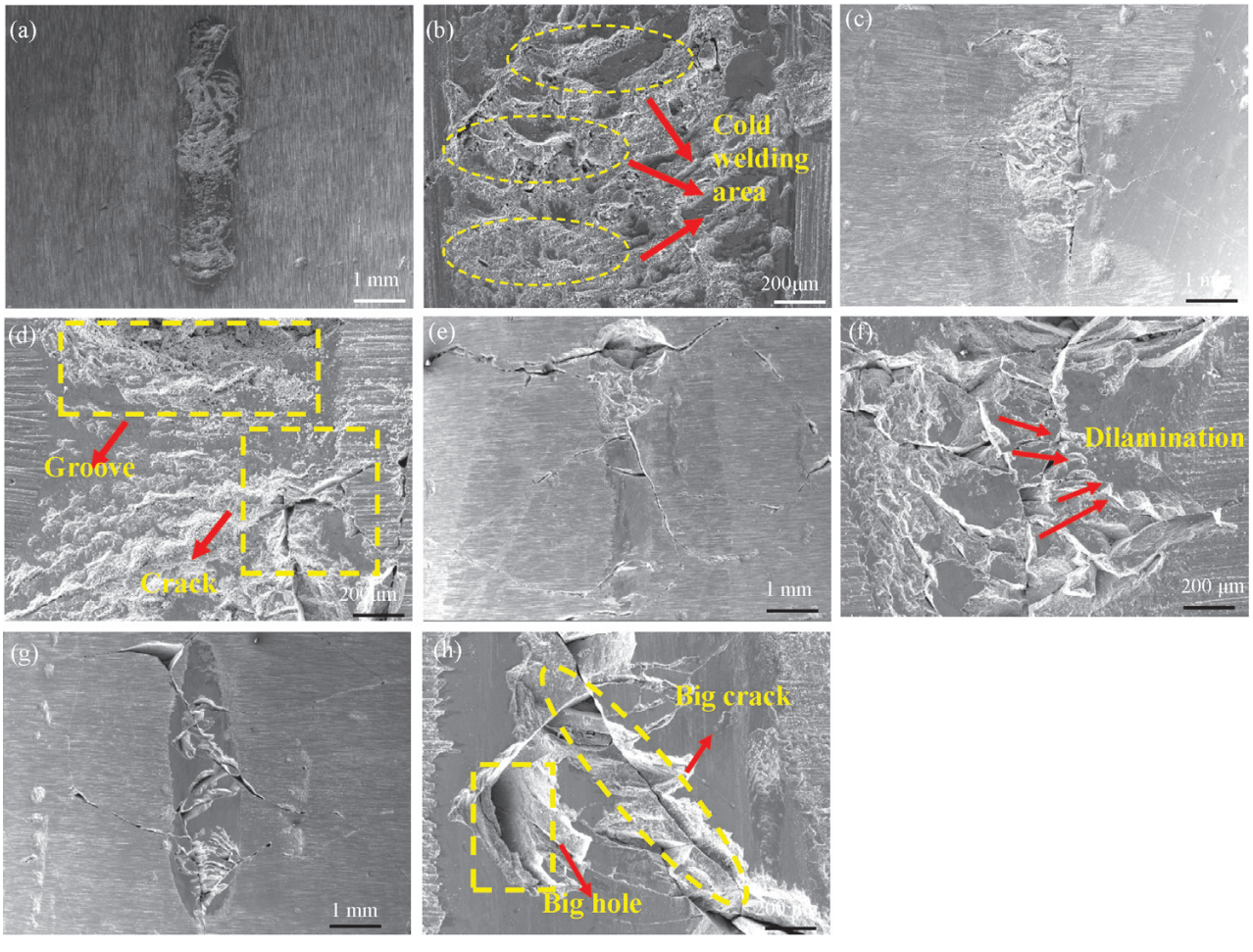

Figure 8: Panorama and local magnification images of the friction surface of amorphous coating after wear test at different temperatures for 30 min: a) and b) RT, c) and (d) 200 °C, e) and f) at 400 °C, g) and h) 600 °C

Table 3: EDS result on the initial amorphous coating and friction surfaces of the coating after wear test at RT, 200 °C, 400 °C and 600 °C for 30 min

Element	Contents of initial coating /(*w*/%)	Contents of RT friction surface /(*w*/%)	Contents of 200 °C friction surface /(*w*/%)	Contents of 400 °C friction surface /(*w*/%)	Contents of 600 °C friction surface /(*w*/%)
O	0.13	12.59	13.30	13.65	21.75
Fe	80.98	44.90	44.85	44.14	39.45
Cr	7.65	20.75	20.20	20.28	18.15
Mo	5.69	15.89	14.22	15.79	13.76
C	5.54	4.24	6.13	5.04	3.42
N	/	0.20	0.30	0.02	0.01
Si	/	1.44	1.01	1.09	3.46

3.2.2 Wear behaviour

The morphologies of the friction surface of the amorphous coating after wear tests at RT, 200 °C, 400 °C and 600 °C for 30 min are shown in **Figure 8**. A large area of cold-welding morphology can be found on the friction surface of the laser-cladded amorphous coating (see **Figure 8a** and **8b**). Adhesive wear was the dominant wear mechanism of the amorphous coating during the RT friction test. During the wear test, a part of material on the top surface of amorphous coating was cut off and adhered to the worn surface of the Si_3N_4 ball due to the hardness of the latter being higher than that of the former. And then the coating and grinding ball were partially bonded and worn together, resulting in cold-welded regions on the friction surface of the amorphous coating. The cold-welding regions decreased, several grooves and cracks appeared in the friction surface of amorphous coating after wear test 200 °C for 30 min as shown in **Figure 8c** and **8d**. The cold-welded regions were almost invisible, and delamination occurred as shown in Figure 8e and 8f. Typical fatigue wear was the main mechanism as friction temperature increased up to 400 °C. A number of delamination, big cracks and holes

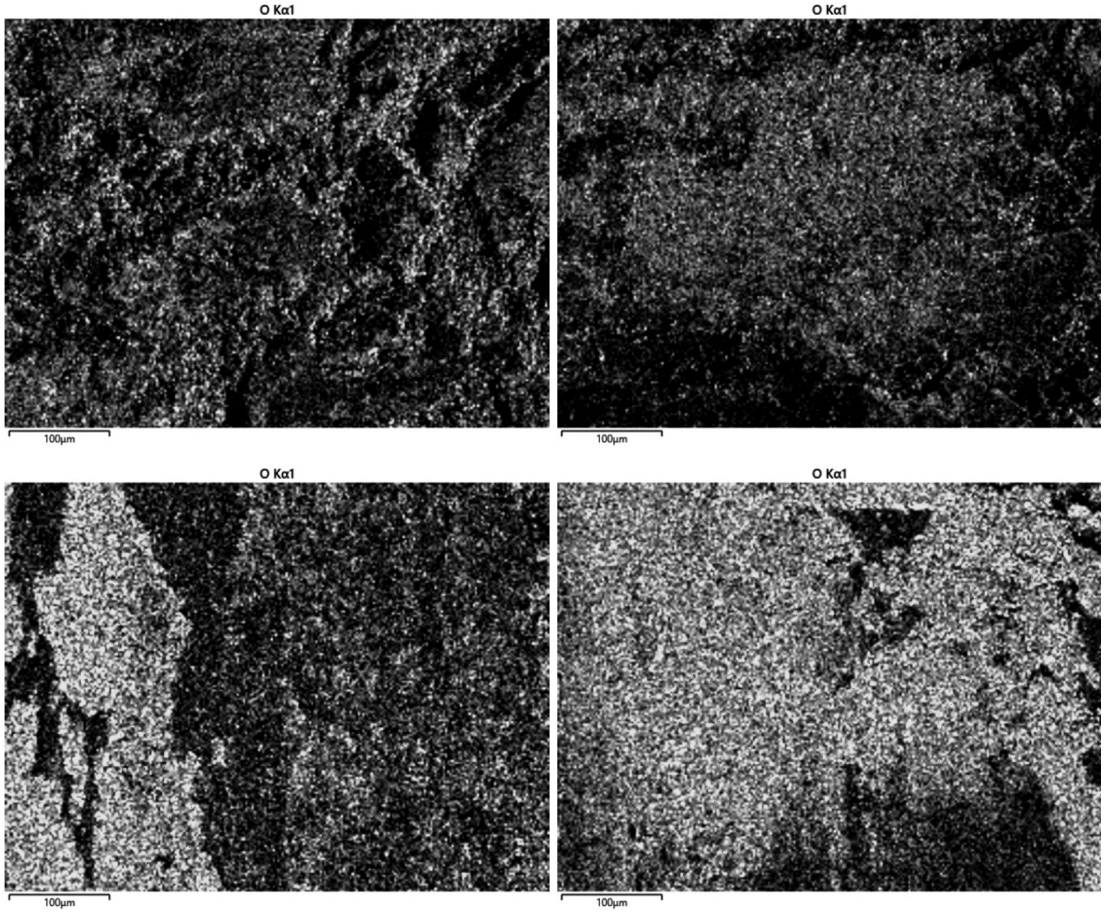

Figure 9: Oxygen distributions on wear traces of iron-based amorphous coatings after wear test at different temperatures for 30 min: a) RT, b) 200 °C, c) 400 °C and d) 600 °C

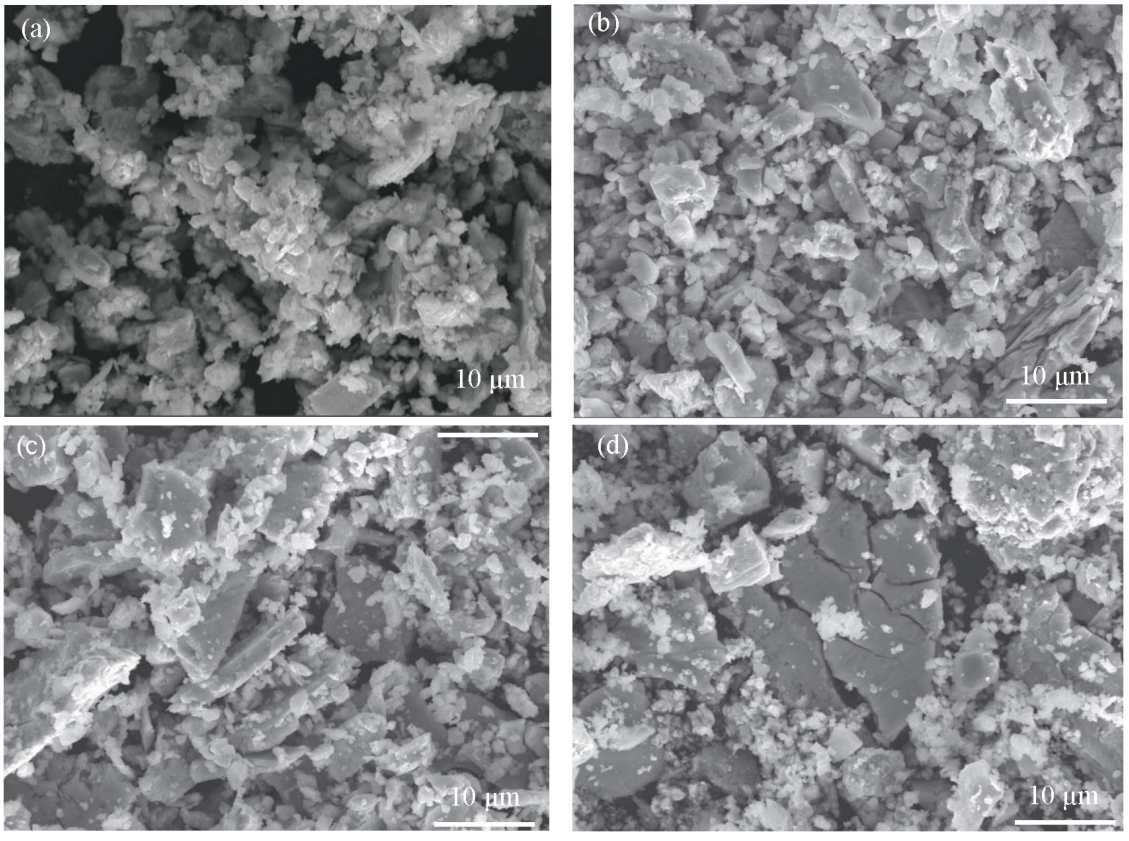

Figure 10: Wear debris collected from iron-based amorphous coatings after wear test at various temperatures: a) RT, b) 200 °C, c) 400 °C and d) 600 °C

appeared, while cold-welded regions completely disappeared in the friction surface (see **Figure 8g** and **8h**).

The EDS results of the initial amorphous coating and the friction surfaces of the coatings after the wear tests at different temperatures for 30 min are shown in **Table 3**. The O content (12.59 %) on the friction surface of coating after wear test at RT is higher than that (0.13 %) of initial amorphous coating due to self-heating from continuous friction. Therefore, oxidation wear occurred throughout the friction experiment. Moreover, the O contents on the friction surfaces gradually increased with the test temperature. From oxygen distributions on the wear traces as shown in **Figure 9**, the oxygen uniformly distributed on the friction surfaces of the coatings, indicating the sufficient reaction of oxygen and metal elements during wear friction. It is notable that several oxygen-rich regions can be seen in **Figure 9c**. This can be ascribed to the coating roughness that decided its surface microscopic height difference, which can cause local temperature rising, and then the local oxygen content increased.

Wear debris collected from the iron-based coatings after the wear test at various temperatures for 30 min can be found in **Figure 10**. It should be noted that the particle size of wear debris increased with the test temperatures. In addition, the portion of plate-like particles of wear debris increased with the test temperature too. Severe abrasion occurred during the 600 °C friction test and as a result complex micro-cracks were formed in the plate-like particles, as shown in **Figure 10d**.

Figure 11 shows the friction coefficient vs. time curves of the amorphous coating under various wear test temperatures. There is a long transitional period in the initial stage of the friction curve of the coating at RT due to the adhesive wear mechanism, which is consistent with the above conclusion of a friction surface morphology. The average friction coefficients of the coatings are shown in **Figure 12**. The average friction coefficients of

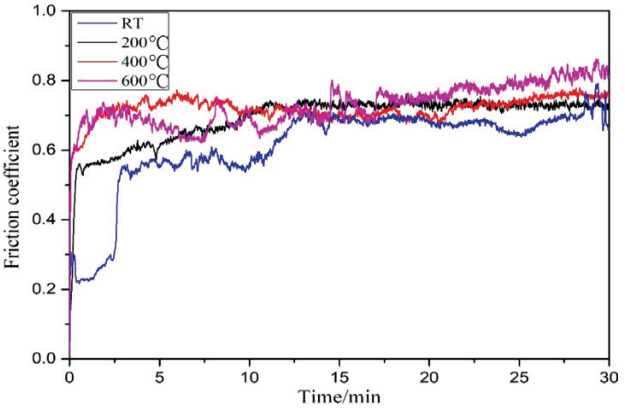

Figure 11: Friction coefficient vs. time curves of the amorphous coating under various test temperatures

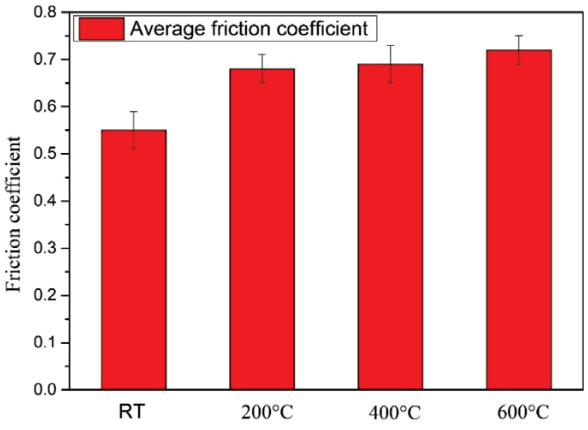

Figure 12: Average friction coefficient of the cladded Fe-based amorphous coatings at different friction temperatures

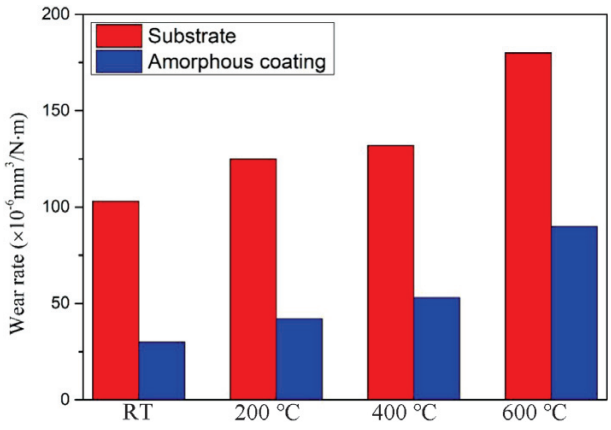

Figure 13: Wear rates of Fe-based amorphous coating and steel substrate under various test temperatures

the coatings at RT, 200 °C, 400 °C and 600 °C are 0.55, 0.68, 0.69, 0.72, respectively. The friction coefficient was gradually increased with the temperature, which can due to the increasing of coating roughness caused by the coating surface oxidation. It is notable that the average friction coefficient was sharply increased when the temperature was elevated from RT to 200 °C. Nevertheless, the friction coefficient difference of coating under 200 °C, 400 °C and 600 °C were relative small. This tendency is completely consistent with the conclusion of oxygen content on the coating friction surface under various wear temperatures.

Figure 13 shows the wear rates of Fe-based amorphous coating and steel substrate after wear tests at various temperatures for 30 min. The wear rates of the amorphous coatings and iron substrate gradually increased with the friction temperatures. Note here, the wear rates of the iron-based amorphous coating were much lower than those of the steel substrate. As a result, the steel substrate can be effectively protected by Fe-based amorphous coatings prepared by laser cladding.

4 CONCLUSIONS

FeCrMoCB amorphous coatings were successfully prepared by laser cladding on 316 stainless-steel substrates. The effects of wear temperature on the wear behavior of Fe-based amorphous coating were discussed. The main results are summarized as follows:

The 1300$HV_{0.1}$ microhardness of the inner coating was the highest among the outer coating, inner coating and bonding area, due to the residual thermal stress during the laser-cladding process.

As the wear temperature rose from RT to 600 °C, the dominating wear mechanism transformed from adhesive wear to fatigue wear, and the wear rate increased from 26×10^{-6} mm^3/N·m to 79×10^{-6} mm^3/N·m.

The laser-cladded Fe-based amorphous coating exhibited much stronger wear performance than the 316 stainless steel, even the wear rate reached even one-third of that of steel, indicating the laser-cladded amorphous coating can protect a steel substrate from wear friction.

Acknowledgment

This work was supported by Natural Science Foundation of Hunan Province of China (Grant No. 2021JJ50025), Key Research and Development Program of Hunan Province (2022GK2030), Natural Science Project of Jiangsu Urban and Rural Construction Vocational College (XJZK22009/206).

5 REFERENCES

[1] M. Yasir, C. Zhang, W. Wang, et al. Wear behaviors of Fe-based amorphous composite coatings reinforced by Al_2O_3 particles in air and in NaCl solution, Materials & Design, 88 (**2015**), 207–213, doi:10.1016/j.matdes.2015.08.142

[2] B. Huang, C. Zhang, G. Zhang, et al. Wear and corrosion resistant performance of thermal-sprayed Fe-based amorphous coatings: A review, Surface and Coatings Technology, 377 (**2019**), 124896, doi:10.1016/j.surfcoat.2019.124896

[3] Y. Wang, K. Y. Li, F. Scenini, et al. The effect of residual stress on the electrochemical corrosion behavior of Fe-based amorphous coatings in chloride-containing solutions, Surface and Coatings Technology, 302 (**2016**), 27–38, doi:10.1016/j.surfcoat.2016.05.034

[4] W. Ning, H. Zhai, R. Xiao, et al. The Corrosion Resistance Mechanism of Fe-Based Amorphous Coatings Synthesised by Detonation Gun Spraying, Journal of Materials Engineering and Performance, 29 (**2020**), 3921–3929, doi:10.1007/s11665-020-04876-w

[5] C. Jiang, W. Liu, G. Wang et al., The corrosion behaviours of plasma-sprayed Fe-based amorphous coatings, Surface Engineering, 34 (**2017**), 634–639, doi:10.1080/02670844.2017.1319647

[6] S. D. Zhang, W. L. Zhang, S. G. Wang, et al. Characterisation of three-dimensional porosity in an Fe-based amorphous coating and its correlation with corrosion behaviour, Corrosion Science, 93 (**2015**), 211–221, doi:10.1016/j.corsci.2015.01.022

[7] N. C. Wu, K. Chen, W. H. Sun, et al. Correlation between particle size and porosity of Fe-based amorphous coating, Surface Engineering, 35 (**2018**), 37–45, doi:10.1080/02670844.2018.1447782

[8] Y. Wang, Z. Z. Xing, Q. Luo, et al. Corrosion and erosion–corrosion behaviour of activated combustion high-velocity air fuel sprayed Fe-based amorphous coatings in chloride-containing solutions, Corrosion Science, 98 (**2015**), 339–353, doi:10.1016/j.corsci.2015.05.044

[9] G. Li, Y. Gan, C. Liu, et al. Corrosion and Wear Resistance of Fe-Based Amorphous Coatings, Coatings, 10 (**2020**), 73, doi:10.3390/coatings10010073
[10] G. Huang, L. Qu, Y. Lu, et al. Corrosion resistance improvement of 45 steel by Fe-based amorphous coating, Vacuum, 153 (**2018**), 39–42, doi:10.1016/j.vacuum.2018.03.042
[11] C. Zhang, Z.-W. Zhang, Q. Chen, et al. Effect of hydrostatic pressure on the corrosion behavior of HVOF-sprayed Fe-based amorphous coating, Journal of Alloys and Compounds, 758 (**2018**), 108–115, doi:10.1016/j.jallcom.2018.05.100
[12] Y. Kang, Y. Chen, Y. Wen, et al. Effects of structural relaxation and crystallization on the corrosion resistance of an Fe-based amorphous coating, Journal of Non-Crystalline Solids, 550 (**2020**), 120378, doi:10.1016/j.jnoncrysol.2020.120378
[13] J. Wu, S. D. Zhang, W. H. Sun, et al. Enhanced corrosion resistance in Fe-based amorphous coatings through eliminating Cr-depleted zones, Corrosion Science, 136 (**2018**), 161–173, doi:10.1016/j.corsci.2018.03.005
[14] M. Yasir, C. Zhang, W. Wang, et al. Enhancement of impact resistance of Fe-based amorphous coating by Al 2 O 3 dispersion, Materials Letters, 171 (**2016**), 112–116, doi:10.1016/j.matlet.2016.02.060
[15] W. Wang, C. Zhang, P. Xu, et al. Enhancement of oxidation and wear resistance of Fe-based amorphous coatings by surface modification of feedstock powders, Materials & Design, 73 (**2015**), 35–41, doi:10.1016/j.matdes.2015.02.015
[16] W. Guo, J. Zhang, Y. Wu, et al. Fabrication and characterization of Fe-based amorphous coatings prepared by high-velocity arc spraying, Materials & Design, 78 (**2015**), 118–124, doi:10.1016/j.matdes.2015.04.027
[17] S. F. Guo, F. S. Pan, H. J. Zhang, et al. Fe-based amorphous coating for corrosion protection of magnesium alloy, Materials & Design, 108 (**2016**), 624–631, doi:10.1016/j.matdes.2016.07.031
[18] H. R. Ma, X. Y. Chen, J. W. Li, et al. Fe-based amorphous coating with high corrosion and wear resistance, Surface Engineering, 33 (2016), 56–62, doi:10.1080/02670844.2016.1176718
[19] J.-j. Xu, J.-j. Kang, W. Yue, et al. High-temperature tribological property of Fe-based amorphous alloy coating, Journal of Non-Crystalline Solids, 573 (**2021**), 121136, doi:10.1016/j.jnoncrysol.2021.121136
[20] C. Li, J. Ding, F. Zhu, et al. Indentation creep behavior of Fe-based amorphous coatings fabricated by high velocity Oxy-fuel, Journal of Non-Crystalline Solids, 503–504 (**2019**), 62–68, doi:10.1016/j.jnoncrysol.2018.09.018
[21] H. Guo, N. C. Wu, Y. L. Zhang, et al. Influence of coating thickness on the impact damage mode in Fe-based amorphous coatings, Surface and Coatings Technology, 390 (**2020**), 125650, doi:10.1016/j.surfcoat.2020.125650
[22] J. Henao, A. Concustell, I. G. Cano, et al. Influence of Cold Gas Spray process conditions on the microstructure of Fe-based amorphous coatings, Journal of Alloys and Compounds, 622 (**2015**), 995–999, doi:10.1016/j.jallcom.2014.11.037
[23] X. Shang, C. Zhang, T. Xv, et al. Synergistic effect of carbide and amorphous phase on mechanical property and corrosion resistance of laser-clad Fe-based amorphous coatings, Materials Chemistry and Physics, 263 (**2021**), 124407, doi:10.1016/j.matchemphys.2021.124407
[24] H. Zhai, X. Li, W. Li, et al. Strategy for improving the wear-resistance properties of detonation sprayed Fe-based amorphous coatings by cryogenic cycling treatment, Surface and Coatings Technology, 410 (**2021**), 126962, doi:10.1016/j.surfcoat.2021.126962
[25] L. M. Zhang, M. C. Yan, S. D. Zhang, et al. Significantly enhanced resistance to SRB corrosion via Fe-based amorphous coating designed with high dose corrosion-resistant and antibacterial elements, Corrosion Science, 164 (**2020**), 108305, doi:10.1016/j.corsci.2019.108305
[26] W. Lu, D. Wang, Q. Wang, et al. Sensitivity of Corrosion Behavior for Fe-Based Amorphous Coating to Temperature and Chloride Concentration, Coatings, 11 (**2021**), 331, doi:10.3390/coatings11030331
[27] H.-z. Wang, Y.-h. Cheng, W. Song, et al. Research on the influence of laser scanning speed on Fe-based amorphous coating organization and performance, Intermetallics, 136 (**2021**), 107266, doi:10.1016/j.intermet.2021.107266
[28] S. L. Wang, Z. Y. Zhang, Y. B. Gong, et al. Microstructures and corrosion resistance of Fe-based amorphous/nanocrystalline coating fabricated by laser cladding, Journal of Alloys and Compounds, 728 (**2017**), 1116–1123, doi:10.1016/j.jallcom.2017.08.251
[29] J. Zhang, M. Liu, J. Song, et al. Microstructure and corrosion behavior of Fe-based amorphous coating prepared by HVOF, Journal of Alloys and Compounds, 721 (**2017**), 506–511, doi:10.1016/j.jallcom.2017.06.046
[30] J. Wu, J. P. Cui, Q. J. Zheng, et al. Insight into the corrosion evolution of Fe-based amorphous coatings under wet-dry cyclic conditions, Electrochimica Acta, 319 (**2019**), 966–980, doi:10.1016/j.electacta.2019.07.058
[31] J. Jiao, Q. Luo, X. Wei, et al. Influence of sealing treatment on the corrosion resistance of Fe-based amorphous coatings in HCl solution, Journal of Alloys and Compounds, 714 (**2017**), 356–362, doi:10.1016/j.jallcom.2017.04.179
[32] H.-z. Wang, Y.-h. Cheng, J.-y. Yang, et al. Influence of laser remelting on organization, mechanical properties and corrosion resistance of Fe-based amorphous composite coating, Surface and Coatings Technology, 414 (**2021**), 127081, doi:10.1016/j.surfcoat.2021.127081
[33] D. Liang, J. Ma, Y. Cai, et al. Characterization and elevated-temperature tribological performance of AC–HVAF-sprayed Fe-based amorphous coating, Surface and Coatings Technology, 387 (**2020**), 125535, doi:10.1016/j.surfcoat.2020.125535
[34] J. Cheng, Q. Zhang, Y. Feng, et al. Microstructure and Sliding Wear Behaviors of Plasma-Sprayed Fe-Based Amorphous Coatings in 3.5 wt.% NaCl Solution, Journal of Thermal Spray Technology, 28 (**2019**), 1049–1059, doi:10.1007/s11666-019-00866-0
[35] Y. Lu, G. Huang, Y. Wang, et al. Crack-free Fe-based amorphous coating synthesized by laser cladding, Materials Letters, 210 (**2018**), 46–50, doi:10.1016/j.matlet.2017.08.125
[36] Q. L. Lu, Y. F. Wang, L. J. Xiao, et al. Effects of La2O3 on Microstructure and Properties of Laser Clad Fe-Based Amorphous Composite Coatings, Materials Science Forum, 749 (**2013**), 583–588, doi:10.4028/www.scientific.net/MSF.749.583
[37] X. Hou, D. Du, K. Wang, et al. Microstructure and Wear Resistance of Fe-Cr-Mo-Co-C-B Amorphous Composite Coatings Synthesized by Laser Cladding, Metals, 8 (**2018**), 622, doi:10.3390/met8080622
[38] L. Xie, Y.-M. Wang, X. Xiong, et al. Comparison of Microstructure and Tribological Properties of Plasma, High Velocity Oxy-Fuel and Detonation Sprayed Coatings from an Iron-Based Powder, Materials Transactions, 59 (**2018**), 1591–1595, doi:10.2320/matertrans.M2018141
[39] L. Xie, Y.-M. Wang, X. Xiong, et al. Effects of Oxygen Fuel Rate on Microstructure and Wear Properties of Detonation Sprayed Iron-Based Amorphous Coatings, Materials Transactions, 59 (**2018**), 1867–1871, doi:10.2320/matertrans.M2018273
[40] Q.-Y. Wang, Y.-C. Xi, Y.-H. Zhao, et al. Effects of laser re-melting and annealing on microstructure, mechanical property and corrosion resistance of Fe-based amorphous/crystalline composite coating, Materials Characterization, 127 (**2017**), 239–247, doi:10.1016/j.matchar.2017.03.011
[41] J. M. Pelletier, L. Renaud and F. Fouquet. Solidification microstructures induced by laser surface alloying influence of the substrate, Materials Science and Engineering, (**1991**) 1283–1287
[42] L. Xie, X. Xiong, Y. Zeng, et al. The wear properties and mechanism of detonation sprayed iron-based amorphous coating, Surface and Coatings Technology, 366 (**2019**), 146–155, doi:10.1016/j.surfcoat.2019.03.028